

Resonance cascading in a ceramic tag for long-range omnidirectional radio-frequency identification communication

Dmitry Dobrykh^{1,*}, Alyona Maksimenko¹, Ildar Yusupov,² Dmitry Filonov,³
Alexey Slobozhanyuk,² and Pavel Ginzburg¹

¹ School of Electrical Engineering, Tel Aviv University, Tel Aviv 69978, Israel

² School of Physics and Engineering, ITMO University, Saint Petersburg 197101, Russia

³ Center for Photonics and 2D Materials, Moscow Institute of Physics and Technology, Dolgoprudny 141700, Russia



(Received 12 September 2023; revised 8 November 2023; accepted 20 November 2023; published 12 December 2023)

Radio-frequency identification (RFID) is a widely used technology for wireless data transfer between tags and readers. Passive ultrahigh-frequency (uhf) RFID architecture is a compromise between cost and performance in numerous retail applications, in which multiple goods must be labeled and simultaneously interrogated from a distance. Furthermore, for robust operation, passive tags must be visible from any direction and for any polarization to compensate for their accidental misalignments with respect to the reader's antenna. Obtaining long-range omnidirectional operation with miniaturized tags remains a challenge, which limits the scope of emerging applications, including the Internet of small things. Here we develop the concept of resonance cascading and demonstrate a new architecture based on a high-index ceramic resonator. Taking advantage of frequency hopping between communication channels, we design several mutually orthogonal spectrally separated dipolar resonances to enable omnidirectional operation inside an RFID frequency band, instead of using traditional single-band quasi-isotropic antennas. As a result, we experimentally demonstrate a compact $28.5 \times 27.5 \times 27$ mm³ device, which can be omnidirectionally interrogated from a distance of over 10 m, which is further than has been previously achieved in the field of long-range omnidirectional uhf RFID tags. The concept of resonance cascading and spectral sharing can be further employed in a variety of wireless communication applications.

DOI: 10.1103/PhysRevApplied.20.064022

I. INTRODUCTION

The ever-growing number of emerging applications impose new demands on data traffic, challenging wireless technologies. Retail, healthcare, logistics, and other niches requiring secure monitoring of numerous goods favor radio-frequency identification (RFID) technology over other existing approaches [1,2]. Forthcoming concepts of the Internet of small things, where low-cost items lacking power resources are expected to become a part of the global network, demand the development of a next generation of passive tags. These devices must be visible from a several-meter distance and support various interrogation scenarios, i.e., provide omnidirectional and all-polarization responses together with a contradictory demand for tag miniaturization.

A typical ultrahigh-frequency (uhf) RFID system is based on a passive tag and an active reader device; the latter initiates the connection and processes data encoded in a modulated backscattered electromagnetic wave. While

RFID communication protocols and transmitted power are subjects of international regulations, application-tailored antenna designs can significantly improve tags' performance [3]. Typical tag antennas are designed to support a broadband dipolar resonance, obtained with meander-shaped strip lines, patches, and several other designs. While broadband resonances grant the tags a certain immunity to environmental changes (e.g., low sensitivity to materials of labeled objects), a dipolar mode cannot provide an omnidirectional response, and it is also subject to polarization mismatch. Many omnidirectional (also known as all-directional or quasi-isotropic) RFID tags have been demonstrated to address this challenge. For example, spherical antennas [4,5], patch antennas [6,7], loop antennas [8], and dielectric resonant antennas [9], as well as several near-omnidirectional realizations [10–18], have been demonstrated. The underpinning operational principle for these devices is overlapping between several resonant modes. However, the key challenge stemming from fundamental laws of electrodynamics is obtaining an omnidirectional response to a linearly polarized excitation [19]. Furthermore, operation at higher-order modes

* dmitryd@mail.tau.ac.il

excited in a subwavelength structure reduces the radiation efficiency, decreasing the RFID reading range. Another essential aspect to consider while designing a tag is the Chu-Harrington limit, which predicts the bandwidth drop if the overall antenna size is reduced [20]. Considering these issues, obtaining a small-footprint device with an omnidirectional all-polarization response remains a challenge. While several quasi-isotropic antenna designs have been reported in the last years [21–30], the objective remains relevant across several wireless communication disciplines.

Here we develop a new approach to overcome these obstacles by using the multichannel property of the RFID communication protocol. Instead of developing an antenna with a quasi-isotropic radiation pattern at a single frequency, we propose to share the spectrum supported by the uhf RFID communication protocol between several cascaded resonances. For example, the uhf RFID band in the United States is 902–928 MHz, comprising 50 channels, 500 kHz each [31]. Frequency hopping between the channels prevents multiple readers from interfering with each other, thus enabling them to interrogate tags in the same area simultaneously.

Our tag is designed to operate at several spectrally separated resonances: each of them falls into one of the adjacent communication channels. Here, the omnidirectional response of the tag is effectively achieved by several individual communication channels, and the fundamental limitations of quasi-isotropic antennas are thus bypassed with the spectral sharing approach. Several (in our case, three) narrowband resonances cover different spatial sectors, which together provide uniform coverage. Furthermore, resonant dipolar resonances will ensure the long-range operation of the hybrid tag. The proposed concept is illustrated in Fig. 1.

The architecture of our tag is based on a high-index ceramic parallelepiped with unequal edges. The structure supports three orthogonal magnetic dipole modes. These modes resonate at different, though very close, frequencies, which fall into the uhf RFID operational bandwidth. A miniature nonresonant metal split ring is placed at a corner of the resonator to obtain coupling with all three orthogonal dipole modes. The ring has a standard RFID chip soldered in the gap. Since the main antenna element is a ceramic resonator, the inductively coupled metal ring picks up the displacement currents in the dielectric and converts them into conduction currents, which drive the chip soldered in the metal ring.

The entire structure can be placed inside a plastic shell, which can be directly attached to a labeled object. We should note that the concept of ceramic RFID tags based on high-index resonators has been developed by us, and several configurations have been reported, e.g., [32–34]. The proposed architecture is conceptually different from the previous reports, and it provides a function that

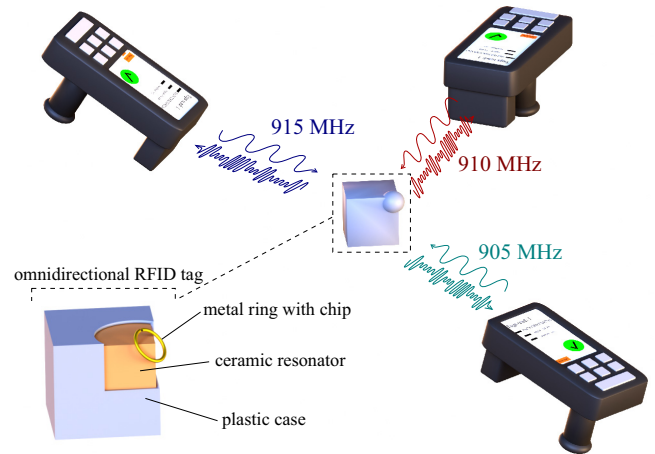


FIG. 1. Operational principle of an omnidirectional long-range ceramic RFID tag. Several orthogonal dipolar modes, resonating at nearby frequencies falling within the uhf RFID band, ensure a uniform spatial response of the tag.

seems to be unachievable without the concept of frequency sharing.

II. ANTENNA DESIGN AND EXCITATION

First, to find the tag's parameters, we performed eigenmode analysis for a cubic dielectric resonator. As the resonator material, we chose $\text{TiO}_2\text{-ZrO}_2$ ceramic with a permittivity $\epsilon_r = 100$ and a dielectric loss tangent of 4×10^{-4} . We used the eigenmode solver in the CST MICROWAVE STUDIO package. The cube edge was found to be $L = 27.5$ mm for the resonator to support three orthogonal dipole magnetic modes TE_{01} at the same frequency of 912 MHz, which is within the 902–928 MHz U.S. uhf RFID band. At the next step, to independently control the frequency of each mode and design proper resonance cascading, we tuned the resonator edges, allowing them to be unequal. Figure 2 demonstrates the vector magnetic field in the cross section through the center of the resonator for three orthogonal magnetic dipole modes TE_{01} calculated by the eigenmode solver. The geometrical parameters of the parallelepiped with unequal edges were $L_x = 28.6$ mm, $L_y = 27.5$ mm, and $L_z = 26.4$ mm.

Next, to calculate the electromagnetic parameters of the tag, we added a feed source—a nonresonant metal ring with an active port. We optimized the ring, using a frequency solver (finite element method) in CST [Fig. 3(a)]. The ring had a diameter d and a discrete port with a complex impedance $Z = 12.7 - 147.8j$ (corresponding to the datasheet impedance of an Impinj Monza R6 RFID chip) placed in the gap. To obtain good impedance matching the tag's antenna was designed (with an inductively coupled resonator and metal ring) to have the complex conjugate impedance to the RFID chip. The impedance matching was realized without additional elements and by adjusting

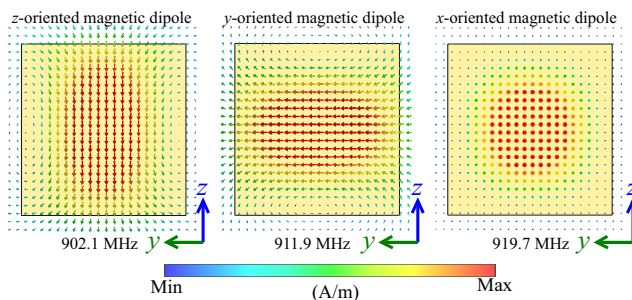


FIG. 2. Numerically calculated vector magnetic field in the cross section through the center of the resonator for three orthogonal magnetic dipole modes TE_{01} .

only the geometrical parameters of the ring and inductive coupling with resonator. This is the same impedance matching approach that we demonstrated in our previous works related to ceramic RFID tags [32–34]. The ring was placed at a corner of the resonator to create inductive coupling with all three orthogonal resonator modes. The final parameters of the tag after all numerical optimizations are summarized in Table I.

Figure 3(b) shows the numerically calculated $|S_{11}|$ spectrum for the optimized omnidirectional ceramic RFID tag. In the range of 902–928 MHz, three impedance-matched resonant peaks can be observed, corresponding to the three orthogonal magnetic dipole modes TE_{01} . The insets show the magnetic field distribution in the cross section through the center of the cylinder. Figure 3(c) demonstrates 3D radiation patterns (realized gain parameter) in a linear scale

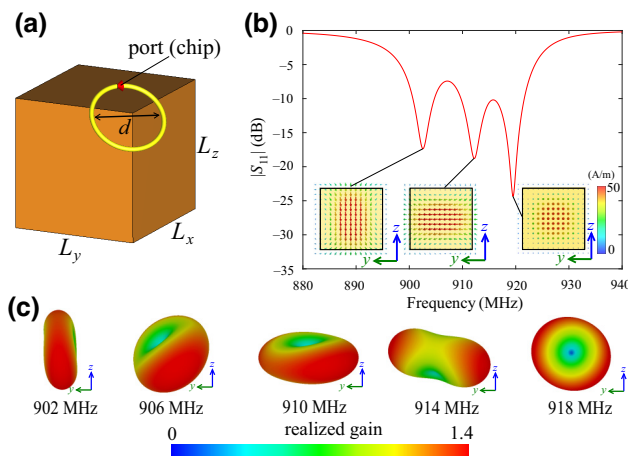


FIG. 3. (a) Omnidirectional long-range ceramic RFID tag. The tag consists of a high-index ceramic resonator (parallelepiped-shaped) and a metal split ring functionalized with an RFID chip. (b) Numerically calculated $|S_{11}|$ spectrum of the proposed ceramic tag. The insets show the vector magnetic field in the cross section through the center of the resonator. (c) Calculated 3D patterns of the realized gain (in a linear scale) at different frequencies in the uhf RFID band.

TABLE I. Parameters of the omnidirectional ceramic RFID tag.

Resonator dimensions (mm)				Ring diameter d (mm)	Ring wire radius w (mm)
L_x	L_y	L_z			
28.6	27.5	26.4		16	1

at different frequencies in the calculated range. At each frequency, a typical dipole radiation pattern is observed. These radiation patterns have different orientations, covering all directions in space and realizing the spectral sharing concept.

The maximum reading range of a passive tag can be calculated with the Friis equation [35],

$$R = \frac{\lambda}{4\pi} \sqrt{\frac{P_t G_{\text{TR}} G_t}{P_{\text{ch}}}}, \quad (1)$$

where P_t is the power transmitted by the reader, G_{TR} is the gain of the reader Tx/Rx antenna, G_t is the realized gain of the tag antenna, P_{ch} is the IC sensitivity, and λ is the operating wavelength. Equation (1), providing the down-link budget, was used to assess the reading range, while the uplink budget is not usually a limiting factor. Of all the parameters included in Eq. (1), we can optimize only the realized gain of the tag, while the transmitted power and gain of the reader's antenna are subject to international regulations. For the 902–928 MHz RFID band, typical effective isotropic radiated power (EIRP) is up to 4 W. Following the Friis equation, we calculated the omnidirectional reading range for the given omnidirectional realized gain of the tag.

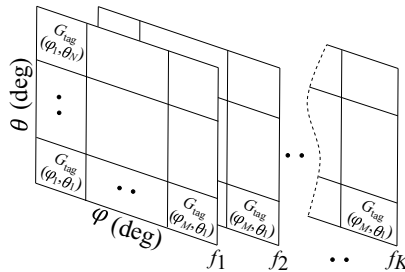
In the following, we describe the postprocessing algorithm used to extract the omnidirectional realized gain. The routine is visually summarized in Fig. 4.

(i) The chosen uhf RFID band (here, 902–928 MHz) is divided into $K = 100$ frequency bins, and for each frequency, an equirectangular projection ($N = 180 \times M = 360$) of the realized gain, initially calculated in spherical coordinate system, is performed—step 1 in Fig. 4. Considering the bin separation, all data are presented as a 3D matrix with $M \times N \times K$ dimensions. In other words, a discretized system of (φ, θ, f) is mapped onto the matrix.

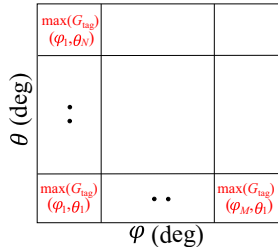
(ii) For each frequency bin, the maximal realized gain is found.

(iii) Since the bandwidth of RFID communication channels is 500 kHz, and in every direction at least one channel must be covered, the minimal value of realized gain in each channel is recorded.

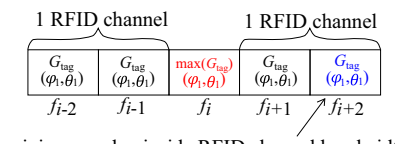
1. 3D matrix of equirectangular projections of tag's realized gain at different frequencies inside uhf RFID band



2. Maximum value of realized gain for each direction in RFID band



3. Maximum value correction due to RFID channel bandwidth



minimum value inside RFID channel bandwidth

4. Equirectangular projection of realized gain inside RFID band

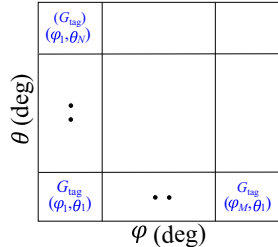


FIG. 4. Postprocessing algorithm used to estimate the maximum omnidirectional realized gain of the proposed ceramic tag.

(iv) We create an equirectangular projection of the tag's maximum realized gain, according to step 3, for each direction in space. The minimal value along all directions is considered the omnidirectional realized gain of the tag.

The results of the postprocessing algorithm are presented in Fig. 5. The equirectangular projections of the tag's realized gain in the 902–928 MHz band were calculated with a frequency step of 250 kHz [Fig. 5(a)]. While

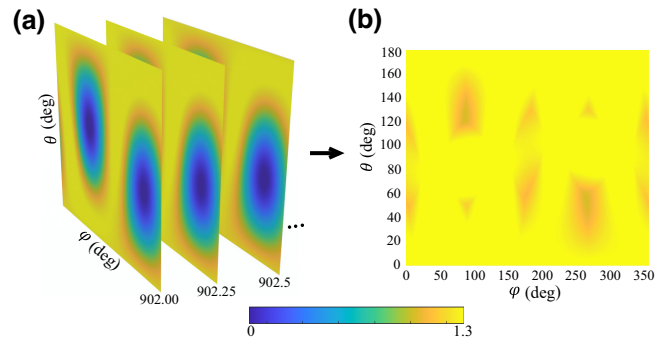


FIG. 5. (a) Equirectangular projections of the tag antenna's realized gain calculated in the 902–928 MHz RFID band. (b) Equirectangular projection of the omnidirectional realized gain obtained with the algorithm described in Fig. 4.

the maximum gain value in Fig. 5(b) is 1.51, which is usual for a dipole resonant antenna, the omnidirectional realized gain is determined as the minimum value $G_t^{\text{omni}} = 0.98$, which limits the reading range in the worst-case direction. Using this value, we estimated the omnidirectional reading range of the proposed ceramic tag,

$$R^{\text{omni}} = \frac{\lambda}{4\pi} \sqrt{\frac{P_t G_{\text{TR}} G_t^{\text{omni}}}{P_{\text{ch}}}} = 16.4 \text{ m.} \quad (2)$$

All the parameters used in the reading range calculation are presented in Table II. We used the sum of transmitted power P_t and reader antenna gain G_{TR} equal to 36 dB, which corresponds to the EIRP limit of 4 W according to the regulations for the U.S. uhf RFID band. Additionally, we used $\lambda = 0.323$ m, which correspond to the highest frequency in the U.S. uhf RFID band. Following the Friis equation, the theoretical omnidirectional reading range of the ceramic tag is 16.1 m, which is one order of magnitude higher than that of the existing omnidirectional RFID tags. A comprehensive comparison with the experimental data is shown in Table III.

While it might be intuitively reasonable that a spectral overlap of modes enables a larger reading range, this approach, however, can spoil the tag's performance. To test this possibility, we performed a parametric study. Let Δf be the spectral distance between the resonances, which can be gradually changed by tuning the resonator dimensions. In Figs. 6(a)–6(c), the possible scenarios are summarized: the peaks can be well separated and fall within the RFID frequency window; they might overlap and thus

TABLE II. Numerical parameters for link budget analysis.

P_t	G_{TR}	P_{ch}	G_t	L^{omni}	λ
1 W	4 (linear)	–20 dBm	0.98 (linear)	16.4 m	0.323 m
30 dBm	(6 dBi)		(–0.08 dB)		

TABLE III. Size and reading distance comparison for omnidirectional RFID tags.

Ref.	Concept	Size (mm)	Reading range (m)	Omnidirectionality
[4]	Electrically small spherical antenna	25 (diameter)	1.32	Omnidirectional
[5]	Electrically small spherical antenna	10 (diameter)	No information	Omnidirectional
[6]	Dual-coil logarithmic patch antenna	28.0 (diameter) \times 3.11 (height)	No information (-5.65 dBi gain)	Nearly omnidirectional
[8]	Metal-mountable planar magnetic loop antenna	$38 \times 38 \times 1.6$	5.6	Nearly omnidirectional
[9]	Electrically small spherical antenna placed in a ceramic powder	$25 \times 25 \times 18$	1.5	Omnidirectional
[12]	Wrapped dipole antenna	$110 \times 19 \times 1.5$	0.3	Nearly omnidirectional
This work	Parallelepiped dielectric resonator antenna with spectrally separated resonances	$28.5 \times 27.5 \times 27$	10	Omnidirectional

hybridize; or be too far from each other, falling outside the allocated frequency range. Figure 6(d) summarizes the realized omnidirectional gain as a function of Δf , demonstrating the clear optimum. When the resonances are too close, they begin to hybridize, decreasing the omnidirectional gain of the tag. While hybridization is beneficial for quasi-isotropic antenna design, it is not optimal for frequency sharing. When the spectral distance between the modes is too large, the omnidirectional gain decreases due to poor circuit matching between the modes, which is essential for radiation in diagonal directions. Furthermore, the resonances should not extend outside the allowed RFID frequency band [Fig. 6(c)]. Consequently, in such a device, optimizing the spectral position of the modes is essential.

The proposed design could be further miniaturized by increasing the permittivity of the resonator. This approach and its limitations are discussed in detail in our previous report [34]. In Fig. 7(a), the proposed RFID tags with different permittivities, namely, 100, 270, and 500, are compared by size. Figure 7(b) demonstrates their spectral responses, which become narrower as the size reduces, in agreement with the Chu-Harrington criterion. We should also note that ceramic elements with permittivities above 100 are susceptible to temperature fluctuations, which might impede circuit matching. Considering those aspects, in the experiment, we used a ceramic with a permittivity of 100.

III. EXPERIMENTAL DEMONSTRATION

After the parametric studies and optimization, we verified the concept experimentally. As a resonator material, ceramic BaLn₂Ti₄O₁₂ was chosen [36]. The permittivity of the material was measured by the vendor to be 101.52 at 1 GHz. The resonator was fabricated

by sintering four identical plates with dimensions of $28.5 \times 27.5 \times 6.75$ mm³. Its final dimensions were $28.5 \times 27.5 \times 27$ mm³.

To find the resonant frequencies of the modes, we used a small loop antenna connected to a 50- Ω port of a vector network analyzer [Fig. 8(a)]. Figure 8(b) shows the measured reflection coefficient $|S_{11}|$. We should note that the impedance matching between the resonator and the 50- Ω port was relatively low because previously we had optimized the structure for the high-impedance RFID chip Impinj Monza R6. This measurement, however, allows the

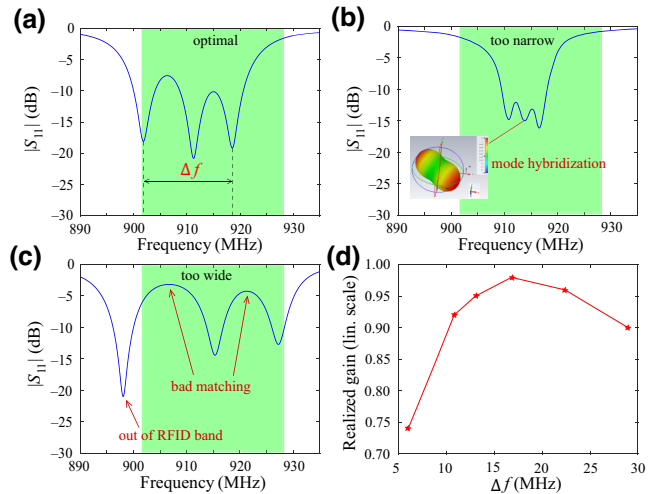


FIG. 6. (a) Numerically calculated $|S_{11}|$ spectrum of the proposed ceramic tag. Δf is the spectral distance between the peaks. (b),(c) $|S_{11}|$ spectra for strong and weak mode overlap, respectively. (d) Tag antenna's omnidirectional realized gain as a function of Δf .

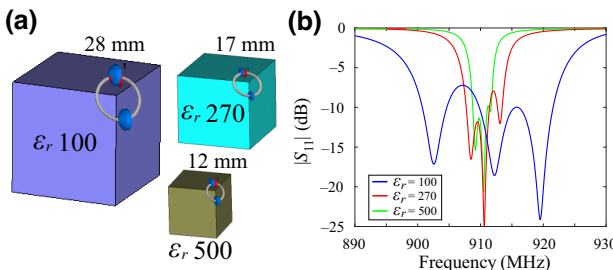


FIG. 7. (a) Numerical models of omnidirectional ceramic RFID tags with different permittivities. (b) Numerically calculated $|S_{11}|$ spectra of ceramic tags with a permittivity of 100 (blue line), 270 (red line), and 500 (green line).

observation of the spectral positions of all three excited modes, which fall within the 894–928 MHz band.

A nonresonant copper ring with an RFID chip, Impinj Monza R6, was placed at a vertex of the ceramic resonator [see inset in Fig. 9(a)]. An RFID reader Impinj R2000, operating at 894–928 MHz, was used to interrogate the tag and measure its radiation pattern in three orthogonal planes. It should be noted that we extended the lower frequency limit from 902 to 894 MHz to cover all three resonances, which do not fall within the standard 902–928 MHz RFID range due to small fabrication inaccuracies (permittivity and geometrical dimensions of the resonator). A linearly polarized (with a polarization parallel to the floor) log-periodic KROKS KM6-600/6000 antenna with a gain of 5.1 dBi at 900 MHz was connected to the reader, which was capable of radiating 30 dBm power. The reader displayed the received signal intensity.

Measurements were made in a large gym to avoid reflections from the walls. The amplitude of the received signal [received signal strength indicator (RSSI) in Fig. 9(b)] was measured with an angular step of 10° in the X - Y , Y - Z , and X - Z planes. The results of interrogation from a 10-m distance are shown in the diagrams in Fig. 9(b). At this distance, we successfully read the tag from all angles

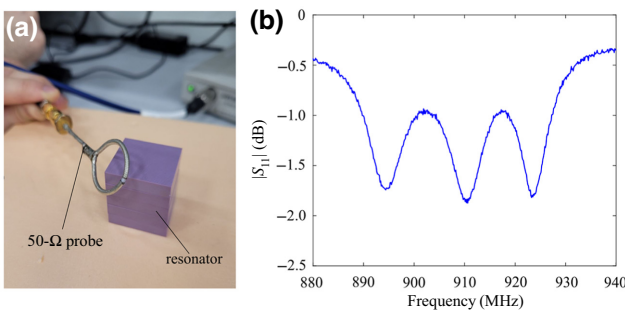


FIG. 8. (a) Photo of the measurement experiment: probing the resonator with a 50- Ω probe. (b) Measured $|S_{11}|$ spectrum of the fabricated ceramic resonator.

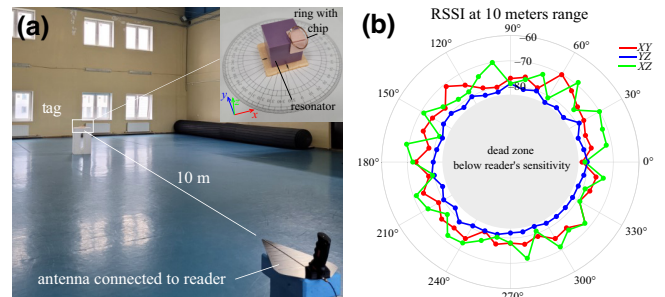


FIG. 9. (a) Photo of the experimental setup with the proposed omnidirectional tag in a large gym. (b) Backscattered signal power (in decibels) at the reader as a function of the tag's angular orientation in three different planes (X - Y , X - Z , and Z - Y).

without identifying any blind spots. The maximum read range of the tag was measured to be 15 m; however, in this case, the tag had blind spots. The reading range can be improved by additional fine tuning and optimization of the tag's parameters (the theoretically achievable reading range is 16 m).

Table III compares the characteristics of several omnidirectional RFID tags with those of the current report. Currently, there are very few experimentally demonstrated omnidirectional tags. The reason is that their fabrication is challenging, and their performances are weak compared with industrial ones. However, our device demonstrates a commercial-level performance, showing that the concept of omnidirectional tags should be reconsidered.

IV. CONCLUSION

A small-footprint long-range omnidirectional ceramic tag has been demonstrated. The design is based on a compact high-index ceramic resonator and an inductively coupled small metal ring functionalized with an RFID IC. A $28.5 \times 27.5 \times 27\text{-mm}^3$ -footprint device was successfully interrogated from a 10-m range in three orthogonal planes, X - Y , Y - Z , and X - Z , without blind spots. At the time of this report, the demonstrated device has the largest omnidirectional reading range for a passive RFID tag. The maximum measured reading range of the tag is 15 m. The proposed architecture combines three essential functions: small footprint, long reading range, and omnidirectional response, which make this design highly attractive for numerous applications, including the Internet of small things and several others.

ACKNOWLEDGEMENTS

This work has been supported by the Russian Science Foundation (Project No. 19-79-10232). The authors thank Lydia Pogorelskaya for her critical reading of the manuscript and useful suggestions.

- [1] X. Zhu, S. K. Mukhopadhyay, and H. Kurata, A review of RFID technology and its managerial applications in different industries, *J. Eng. Technol. Manag.* **29**, 152 (2012).
- [2] R. Weinstein, RFID: A technical overview and its application to the enterprise, *IT Prof.* **7**, 27 (2005).
- [3] K. V. S. Rao, P. V. Nikitin, and S. F. Lam, Antenna design for UHF RFID tags: A review and a practical application, *IEEE Trans. Antennas Propag.* **53**, 3870 (2005).
- [4] H.-K. Ryu, G. Jung, D.-K. Ju, S. Lim, and J.-M. Woo, An electrically small spherical UHF RFID tag antenna with quasi-isotropic patterns for wireless sensor networks, *IEEE Antennas Wireless Propag. Lett.* **9**, 60 (2010).
- [5] A. Bou-El-Harmel, A. Benbassou, and J. Belkaid, Design and development of a new electrically small 3D UHF spherical antenna with 360° of opening angle in the whole space for RFID, WSN, and RSN applications, *Int. J. Antennas Propag.* **2016**, 1 (2016).
- [6] J. H. Low, P. S. Chee, and E. H. Lim, in *Proceedings - 2022 RFM IEEE International RF and Microwave Conference* (2022).
- [7] S. Y. Ooi, P. S. Chee, E. H. Lim, J. H. Low, and F. L. Bong, A zeroth-order slot-loaded cap-shaped patch antenna with omnidirectional radiation characteristic for UHF RFID tag design, *IEEE Trans. Antennas Propag.* **71**, 131 (2023).
- [8] S. R. Lee, W. H. Ng, E. H. Lim, F. L. Bong, and B. K. Chung, Compact magnetic loop antenna for omnidirectional on-metal UHF tag design, *IEEE Trans. Antennas Propag.* **68**, 765 (2020).
- [9] A. Mikhailovskaya, I. Yusupov, D. Dobrykh, S. Krasikov, D. Shakirova, A. Bogdanov, D. Filonov, and P. Ginzburg, Omnidirectional miniature RFID tag, *Appl. Phys. Lett.* **119**, 033503 (2021).
- [10] Y. H. Lee, E. H. Lim, F. L. Bong, and B. K. Chung, Loop-fed planar inverted-L antennas (PILAs) for omnidirectional UHF on-metal tag design, *IEEE Trans. Antennas Propag.* **68**, 5864 (2020).
- [11] N. Tariq, M. A. Riaz, H. Shahid, M. J. Khan, M. S. Khan, Y. Amin, J. Loo, and H. Tenhunen, Orientation independent chipless RFID tag using novel trefoil resonators, *IEEE Access* **7**, 122398 (2019).
- [12] Y. Chen, Y.-H. Su, H. Kuan, and S. J. Chang, Design of near omnidirectional UHF RFID tag with one-off seal function for liquid bottles, *Microwave Opt. Technol. Lett.* **55**, 375 (2013).
- [13] H. Wang, Y. Wang, Y. Liu, and W. Yu, in *ISAPE 2008 - 8th Int. Symp. Antennas, Propag. EM Theory Proc.* (2008), pp. 118.
- [14] L. Pazin, A. Dyskin, and Y. Levitan, Quasi-isotropic X-band inverted-F antenna for active RFID tags, *IEEE Antennas Wireless Propag. Lett.* **8**, 27 (2009).
- [15] L. Liang and S. V. Hum, A low-profile antenna with quasi-isotropic pattern for UHF RFID applications, *IEEE Antennas Wireless Propag. Lett.* **12**, 210 (2013).
- [16] F. Babaeian and N. C. Karmakar, in *2020 27th International Conference on Telecommunications (ICT)* (IEEE, 2020), pp. 1–5.
- [17] M. El Bakkali, M. El Bekkali, G. K. Sodhi, P. Singh, and L. Kansal, in *Proc. - IEEE 2021 Int. Conf. Comput. Commun. Intell. Syst. ICCSIS 2021* (2021), pp. 782.
- [18] H. Liu, J. Liu, and J. Song, in *2022 Int. Appl. Comput. Electromagn. Soc. Symp. ACES-China 2022* (2022).
- [19] H. Matzner and K. T. McDonald, Isotropic Radiators, (2003).
- [20] R. F. Harrington, *Time-Harmonic Electromagnetic Fields*, 2nd ed. (Wiley-IEEE Press, New York, 2001).
- [21] Y. Wang, M. C. Tang, S. Chen, L. Li, D. Li, K. Z. Hu, and M. Li, Design of low-cost, flexible, uniplanar, electrically small, quasi-isotropic antenna, *IEEE Antennas Wireless Propag. Lett.* **18**, 1646 (2019).
- [22] S. M. Radha, G. Shin, W. Kim, S. I. H. Shah, and I. J. Yoon, Design and verification of an electrically small, extremely thin dual-band quasi-isotropic antenna, *IEEE Antennas Wireless Propag. Lett.* **19**, 2482 (2020).
- [23] R. Wang, J. J. Ma, C. S. Chen, B. Z. Wang, and J. Xiong, Low-profile implementation of U-shaped power quasi-isotropic antennas for intra-vehicle wireless communications, *IEEE Access* **8**, 48557 (2020).
- [24] Y. Xu, Y. Zhu, S. Wen, and Y. Dong, Planar quasi-isotropic antenna and its implementation of filtering response, *IEEE Antennas Wireless Propag. Lett.* **20**, 2407 (2021).
- [25] J. W. Luo, Y. M. Pan, S. Y. Zheng, and S. H. Wang, A planar angled-dipole antenna with quasi-isotropic radiation pattern, *IEEE Trans. Antennas Propag.* **68**, 5646 (2020).
- [26] Y. Wang and S. Yan, A compact in-band full duplexing antenna with quasi-isotropic radiation pattern for IoT-based smart home and intravehicle wireless communication applications, *IEEE Internet Things J.* **9**, 16689 (2022).
- [27] J. Kim, J. Park, A. Abdelmottaleb Omar, and W. Hong, A symmetrically stacked planar antenna concept exhibiting quasi-isotropic radiation coverage, *IEEE Antennas Wireless Propag. Lett.* **19**, 1390 (2020).
- [28] H. Liao, Q. Zhang, M. A. Karimi, Y. H. Kuo, N. Mishra, and A. Shamim, An additively manufactured 3-D antenna-in-package with quasi-isotropic radiation for marine animals monitoring system, *IEEE Antennas Wireless Propag. Lett.* **18**, 2384 (2019).
- [29] Y. Guo, Y. Li, J. Wang, L. Ge, Z. Zhang, M. Chen, Z. Li, B. Ai, and R. He, A 3D printed nearly isotropic Luneburg lens antenna for millimeter-wave vehicular networks, *IEEE Trans. Veh. Technol.* **71**, 1145 (2022).
- [30] A. Kumar, C. S. Rai, and M. K. Khandelwal, in *Proc. IEEE Madras Sect. Int. Conf. 2021, MASCON 2021* (2021).
- [31] D. Dobkin, *The RF in RFID: Passive UHF RFID in Practice* (Elsevier, Oxford, 2007).
- [32] D. Dobrykh, I. Yusupov, S. Krasikov, A. Mikhailovskaya, D. Shakirova, A. A. Bogdanov, A. Slobozhanyuk, D. Filonov, and P. Ginzburg, Long-range miniaturized ceramic RFID tags, *IEEE Trans. Antennas Propag.* **69**, 3125 (2021).
- [33] I. Yusupov, D. Dobrykh, D. Filonov, A. Slobozhanyuk, and P. Ginzburg, Miniature long-range ceramic on-metal RFID tag, *IEEE Trans. Antennas Propag.* **70**, 10226 (2022).
- [34] D. Dobrykh, I. Yusupov, P. Ginzburg, A. Slobozhanyuk, and D. Filonov, Self-aligning roly-poly RFID tag, *Sci. Rep.* **12**, 1 (2022).
- [35] P. V. Nikitin and K. V. S. Rao, Theory and measurement of backscattering from RFID tags, *IEEE Antennas Propag. Mag.* **48**, 212 (2006).
- [36] E. A. Nenasheva, O. N. Trubitsyna, N. F. Kartenko, and O. A. Usov, Ceramic materials for use in microwave electronics, *Phys. Solid State* **41**, 799 (1999).